FINAL REPORT

ANALYSIS OF DATA FROM THE YOKOHAMA DENSE ARRAY AND ITS APPLICABILITY FOR UNDERSTANDING VARIABILITY OF GROUND MOTION IN SEATTLE

Award: 03HQGR0053

Element II: Evaluate Urban Hazard and Risk

Ralph J. Archuleta

Institute for Crustal Studies
University of California, Santa Barbara

Research supported by the U. S. Geological Survey (USGS), Department of Interior, under USGS award number 03HQGR0053. The views and conclusions contained in this document are those of the authors and should not be interpreted as necessarily representing the official policies, either expressed or implied, of the U. S. Government.

Award: 03HQGR0053

ANALYSIS OF DATA FROM THE YOKOHAMA DENSE ARRAY AND ITS APPLICABILITY FOR UNDERSTANDING VARIABILITY OF GROUND MOTION IN SEATTLE

Ralph J. Archuleta
Institute for Crustal Studies
University of California, Santa Barbara 93106
Phone: 805-893-8441
FAX: 805-893-8649
Email: ralph@crustal.ucsb.edu

TECHNICAL ABSTRACT

Estimation of the spatial variation of frequency-dependent site amplification factors has been investigated based on the data of the very dense Yokohama array network. First, we took two groups of events based on its focal depth and calculated ground motion parameters, such as PGA, PGV, and Duration. The statistical analysis of the parameters showed that the spatial variation of each parameter seems to be correlated with the distribution of average shear wave velocities for upper 30m. Next, using a nonlinear algorithm, we inverted the data from the borehole accelerometers to determine site response, source parameters, and path attenuation parameters. The source parameters of the earthquakes are consistent with those determined in previous studies. Stress drops for events near Yokohama are about 100 bars. For deep events we find that the path attenuation is almost independent of frequency; there is a stronger dependence on frequency for events with depths less than 20 km. Having determined the critical parameters of the path and the source we directly computed the frequency dependent site response for all 150 surface stations as follows: for 17 deep events and four shallow events we computed the predicted spectrum based on our knowledge of the path and source parameters gained from inversion of the borehole records. For each site and for each event we calculated the misfit between the observed and predicted amplitude spectrum and then averaged over all the events to determine a site response for each of the 150 surface stations. For frequencies less than 3.0 Hz the average site response correlates with average shear wave velocities for upper 30m. Because of the density of the stations we could quantitatively evaluate the site response as a function of separation distance and frequency. To do this we defined a site correlation function. Contours of this function for station pairs separated by distances less than 1.0 km indicate that site amplification can be predicted within 20%, especially for frequencies less than 2.0 Hz and within a factor of 2.5 over all frequencies and separation distances up to 1 km.

Introduction

The effect of local site conditions on earthquake ground motions can be documented as far back as the 1906 earthquake [1]. Borcherdt [2] was the first to compute spectral amplification by taking ratios of the Fourier amplitude spectrum of soil site to a rock site. This work was extended to cover a wider range of site conditions and events [3] and concluded that the site response map "provides a crude form of seismic zonation for the region …" Recent earthquakes such as the 1994 Northridge and 1995 Hyogo-ken Nanbu (Kobe) have clearly demonstrated that site effects play a major role in damaging ground motion, e.g., [4], [5], [6], [7]. One of the primary engineering questions is whether knowing the site response can reduce the uncertainty in predicting ground motion from future events. Stewart and Baturay [8], [9] show that ground response analysis can improve the accuracy of ground motion predictions relative to attenuation relations for soil sites. The SCEC (Southern California Earthquake Center) Phase III Working Group [10] found that the average shear wave velocity in the upper 30m delineated different amplification factors. Likewise they found that the depth to basin was highly correlated to amplification but cautioned that the depth of the basin might be substituting for some other site attribute. The effect of coherency on site response has been well studied empirically and analytically, e.g., [11], [12], [13] and [14]. These studies have demonstrated how phase differences in the time history can create differences in the site response as a function of distance between sites. A complementary and basic question is how the site amplification itself varies from site to site. In practice we need to separate effects that are event-to-event from those that are site-to-site. Quantifying the spatial variation of site response from event-to-event and site-to-site requires a dense set of stations as well as multiple events. In order to evaluate spatial variation, some seismic array systems have been developed, e.g., [15]. Especially, the Yokohama high-density strong ground motion network constructed by the city of Yokohama has 150 stations within very small area. The analysis of this very unique array data made it possible to estimate the spatial variation of site response within very narrow area, and it can be applicable to other general cases. In this study, we first have analyzed ground motion parameters statistically and compared to the geotechnical parameters related to the structure at each site. Next, to quantify the spatial variation of site response, we computed site response for each of the 150 stations. Using the nine borehole stations we nonlinearly invert for the source and path parameters for each event. The site response for each surface station is easily computed as the difference between the average computed spectrum and the average observed spectrum. Finally, we introduced a site correlation factor that tries to estimate how site amplification changes with station separation.

Yokohama Seismic Array

The city of Yokohama, located southwest of Tokyo, has the densest array of strong motion accelerometers anywhere in the world [16], [17], [18]. The array has 150 surface stations with 3-component accelerometers and nine borehole sites with instruments at depths between 16 and 69 m. The surface stations cover an area 434 km^2 that is approximately 25 km x 20 km with spacing on the order of 2 km with many sites much closer together. We analyzed data from 29 earthquakes (Table 1) ranging in magnitude M_W 4.0–7.3, depths in the range 3–430 km and azimuthal coverage of nearly 270˚ (Figure 1). The Yokohama seismic array was designed to provide real-time assessment of damage and to provide strong-motion data for improving construction that would make Yokohama more resistant to earthquake damage [16]. The array, completed in May 1997, consists of 150 three-component surface stations supplemented by 9 borehole stations (Figure 2). Each station has descriptions of the local P and S wave velocities as

well as the lithology for the near surface (10–70 m). The 9 borehole stations range in depth from 20 to 70 m, approximately; the surface station spacing is approximately 2 km with many stations even closer. The array covers geological settings ranging from reclaimed land to late tertiary

Table 1: Location and Magnitudes of Earthquakes Recorded on Yokohama Array

	Event	Lat.	Long.	Depth (km)	Mw	Moment (Nm)	No. Surface Stns.	No. Boreholes
1	1/14/98	35.59	140.24	76	4.9	2.28E+16	149	0
2	1/16/98	35.21	140.25	57	4.5	5.36E+15	148	0
3	4/26/98	34.96	139.17	5	4.7	3.46E+16	137	0
4	5/3/98	34.95	139.18	3	5.5	2.34E+17	149	9
5	5/16/98	34.97	139.94	74	4.7	1.49E+16	150	9
6	6/14/98	35.44	140.76	51	5.7	3.58E+17	146	0
7	8/29/98	35.6	140.05	67	5.3	9.80E+16	149	9
8	11/8/98	35.61	140.05	78	4.7	1.36E+16	150	9
9	11/28/98	35.63	140.10	67	4.3	3.29E+15	144	9
10	12/3/98	35.61	140.04	67	4.4	3.87E+15	142	9
11	3/26/99	36.45	140.62	58	5.1	4.55E+16	98	0
12	4/25/99(18:00)	35.52	140.30	92	4.4	4.49E+15	144	7
13	4/25/99(21:00)	35.46	140.63	58	5.2	6.24E+16	104	5
14	5/7/99	35.22	138.35	20	4.8	1.56E+16	75	0
15	5/22/99	35.45	139.19	23	4.1	1.61E+15	148	9
16	7/15/99	35.92	140.46	56	5.1	5.33E+16	126	6
17	8/9/99	35.83	139.96	116	4.6	8.17E+15	106	9
18	8/11/99	35.4	139.83	62	4.0	9.93E+14	133	6
19	9/13/99	35.57	140.20	77	5.3	1.08E+17	150	9
20	2/11/00	35.5	139.05	18	4.2	2.29E+15	149	9
21	4/10/00	35.19	140.07	55	4.7	1.26E+16	142	9
22	6/3/00	35.68	140.72	48	6.1	1.72E+18	147	9
23	8/6/00	28.86	140.07	430	7.3	1.20E+20	142	9
24	8/27/00	35.76	140.14	77	4.6	9.31E+15	126	8
25	9/29/00	35.5	139.70	90	4.8	1.83E+16	148	9
26	9/18/01	35.4	139.80	51	4.5	5.59E+15	144	9
27	12/8/01	35.5	139.10	30	4.5	6.13E+15	146	9
28	11/3/02	38.9	142.10	50	6.4	3.87E+18	97	6
29	3/13/03	36.1	139.90	50	4.9	2.34E+16	133	8

These parameters were determined by National Institute for Earth Science and Disaster Prevention (NIED), Tsukuba, Japan except for the seismic moment of Event 23, which was determined by Kikuchi and Yamanaka [19].

sediments (soft rock) (Figure 3). There are more than 1400 borehole logs of the lithology throughout Yokohama. By correlating measured shear wave velocities at the 150 accelerometer sites with the local geology the four basic lithological units are given estimated velocities for the near surface: reclaimed land, 120–190 m/s; Holocene sediments, 140-400 m/s; Pleistocene sediments, 130-500 m/s and late Tertiary sediments, > 700 m/s [18]. However, when averaged over the upper 30 m, most of the area has an average S–wave velocity near 300 m/s. The basin

structure underlying Yokohama is part of the greater Kanto basin. The contours of the P wave velocity indicate that Yokohama city sits above the western boundary of the deepest part of the basin, approximately 3.5–4.0 km [20], [21]. We assumed the base has a Poisson ratio of 0.25, an S-wave velocity of 3.1 km/s with a corresponding P-wave velocity 5.37 km/s.

Such a dense array made it possible to document the spatial variation of different measures of ground motion, e.g., peak ground acceleration (PGA), (Figure 3). With many different earthquakes it was possible to quantify statistically the variation of such ground motion parameters and to correlate such parameters not only with surficial geology but also with subsurface features such as shear wave velocity for upper 30m. While PGA is an obvious parameter to examine, there are many other parameters that can provide important engineering information such as cumulative absolute velocity, response spectrum intensity, Arias intensity, duration, etc [22]. We analyzed these parameters statistically for the different events and tried to correlate with shear wave velocity. With many of the events being located in approximately the same region (Figure 1) we took advantage of averaging over the different events.

Statistical Analysis of Ground Motion Parameters

The site response has for the nine borehole stations had been determined previously from six earthquakes [17]. Seven of nine borehole site responses were fairly well predicted by the velocity logs. Seven earthquakes recorded on all the stations have been used to determine site response, in particular to determine the fundamental period and the amplitude of the fundamental period at each site [23]. They found that the theoretical site response, based on the local logs of *in situ* P and S-wave velocities, predicted almost 95% of the peak amplitudes and periods within a factor of two. For all these 29 events we have computed the same ground motion parameters that are given in the headings of Table 2. To illustrate some of our results we take three groups of earthquakes, we used the data from 21 events with borehole records. Since the hypocenters for events 23 and 28 are too far from this array we did not use the data from these events. To illustrate some of our results, we take three groups of earthquakes: 4 shallow events, 7 deep events ($4.0 \leqq M \leqq 4.6$), and 10 deep events ($4.7 \leqq M \leqq 5.3$) based on the focal depth and magnitude (Table 1) With each group we have tried to examine the relationship of the ground motion parameters—Cumulative Absolute Velocity (CAV), Spectral Intensity (SI) Arias Intensity (AI), Peak Ground Acceleration (PGA), Peak Ground Velocity (PGV) and Duration (Dur)—with the average shear wave velocity for upper 30 m (ASV30). We only use 2 horizontal components and took vector summation of them, while taking average of them only for duration. We divided the ASV30 into 7 bins: 0-200 m/s (12 stations), 200-250 m/s (11), 250-300 m/s (19), 300-350 m/s (35), 350-400 m/s (35) and 400-700 m/s (17). The value of ASV30 is based on logs for depths for each station. We derived a mean value of the ground motion parameter and the standard deviation of the mean using the number of stations in each velocity bin. The results are shown in Figures 4a,b. The most obvious result of this work is that within a group of shallow events and larger deep events, there is a clear trend of these three parameters with the ASV30 except for AI and PGA. However, the parameters seem to be independent of the ASV30 except for SI and Dur for small deep events. Specially, within these parameters, SI and Dur show very good correlation with ASV30. (Correlation coefficients for SI are -0.82 for shallow, -0.62 for smaller deep, and -0.93 for larger deep events, and for Dur are -0.86 for shallow, -0.76 for smaller deep, and -0.85 for larger deep events). On the other hand, PGA, AI showed little correlation for all three groups.

To examine if there might be a spatial correlation with ASV30 that would not show up in these figures we have contoured the averaged variables on maps of ASV30 for these events in

Figures 5a, b. Although it is too preliminary to draw any conclusions, there are certain areas of the city where SI, AI, CAV seem to peak independent of event group. And these are the same areas that show the low velocity area at the north part of the city. These trends agree with the results of statistic analysis. The further calculations are needed to validate these conclusions about the spatial correlation that accounts for a single variable such as shallow shear wave velocity. The additional data from the Yokohama array offer chance to quantify spatial variability of ground motion over a wide range of distances for a variety of source-site geometries of the city where seems to peak for each of the events. The further calculations are needed to validate these conclusions about the spatial correlation that accounts for a single variable such as shallow shear wave velocity. The additional data from the Yokohama array offer chance to quantify spatial variability of ground motion over a wide range of distances for a variety of source-site geometries.

Site Response

In a previous section, some ground motion parameters are estimated. However, those parameters include not only site response, but source and path effects. To estimate the spatial variation of site response more quantitatively, it is necessary to separate the site response from the observed records. The observed ground motion generally can be expressed a convolution of the source, path and site. To estimate the spatial variation of site response, it is necessary to separate those three quantities analytically. Because of the unique data set we have to devise a method for separating these quantities. In the frequency domain, we can write the convolution as a multiplication: $A(f) = S(f)P(f)Site(f)$ where f is frequency, $A(f)$ is the spectrum of the recorded ground motion, $P(f)$ is the path effect, which is modeled as frequency dependent attenuation $Q(f) = Q_o f^{\gamma}$ in this study, and $Site(f)$ is the site response. However, the source has a nonlinear dependence on the corner frequency assuming an f^2 model: $S(f) = CM_o(2\pi f)^2 f_c^2 \Big/ \left(f^4 + f_c^4\right)^{0.5}$ where C is a constant that depends on distance from source to site, radiation parameter of the source and material parameters; M_o is seismic moment that is related to the size of the earthquake and f_c is the corner frequency that controls the high frequency shape of the spectrum [24], [25]. The path effect also has a nonlinear dependence on frequency if we assume that the attenuation parameter (damping) has a power law dependence on frequency $Q(f) = Q_o f^{\gamma}$. Of the the corner frequency that controls the high frequency shape of the spectrum [24], [25]. The path effect also has a nonlinear dependence on frequency if we assume that the attenuation parameter damping has a power law dependence on frequency $Q(f) = Q_o f^{\gamma}$. Of the 21 events used by statistical analysis used in the previous section, we picked 13 events (9 deep events and 4 shallow events) that are best recorded at borehole stations to be used as reference events. The record section used for this inversion starts 1.0 s before the direct S-wave arrival and has a length 10.0 s. We use the data to estimate: the source parameters (M_o, f_c), the attenuation parameters for the path (Q_o, γ) and the frequency dependent site effect $Site(f)$. The quality factor Q (equivalent to 1/(2xdamping) in engineering terms) is assumed to be constant for frequencies less than 1.0 Hz while having a power law relation for frequencies greater than 1.0 Hz. Because of the spectrum is not linearly related to the corner frequency and the attenuation parameter γ, we need to solve a nonlinear problem. We use a Heat Bath algorithm [26] to invert for the parameters: M_o, f_c, Q_o, γ and the frequency dependent site response. The overall approach is iterative as explained later. We used only the data from nine deep events recorded on the borehole accelerometers. Initially we assume that the borehole response is a constant. Under this

assumption we invert the data for all nine events to determine M_o, f_c, Q_o, γ. The difference between the observed and predicted spectrum is taken as our first estimate of the site response. Our next step is to use this estimate of the site response and invert for M_o using only the spectrum f ≤ 1.0 Hz. With this estimate of the seismic moment and the site response we again invert all of the data to find f_c, Q_o, γ. This produces the second estimate of the site response as the difference between the predicted (based on the current values of M_o, f_c, Q_o, γ) spectrum and the observed spectrum. We iterate this procedure until the residuals between observed and predicted spectra are negligible. Thus we derive a frequency dependent site response for each of the borehole stations as well as solving for the path parameters Q_o, γ,. Now that we have stable values of the site response and path effect, we invert the data from each of the 17 deep events with borehole data to find M_o, f_c (Table 2, Figure 6). The same procedure is applied to four shallow events, but there are differences in the material properties of the medium between the deep and shallow events. From this analysis we find a frequency dependent Q for deep events $Q(f) = 284 f^{0.06}$ which is almost independent of frequency. However for the shallow events we find stronger frequency dependence, $Q(f) = 74 f^{0.28}$. The quality of the inversion procedure is illustrated in Figure 7 where we plotted the predicted spectrum for nine borehole stations. The borehole response at each station is also shown. The agreement between the observed and predicted spectrum from 0.5-30 Hz is excellent (Figure 7).

Table 2: Source Parameters Derived by Inversion

Event	Date	Mo [Nm]	M_W	f_c[Hz]	Stress Drop (bars)
4*	5/3/98	2.08E+16	4.8	1.9	216
5	5/16/98	2.16E+16	4.9	2.4	268
7	8/29/98	1.22E+17	5.4	1.2	195
8	11/8/98	2.56E+16	4.9	2	195
9	11/28/98	5.04E+15	4.4	3	131
10	12/3/98	7.23E+15	4.5	2.5	101
12	1999/4/25_1	6.95E+15	4.5	3.8	345
13	1999/4/25_2	3.76E+16	5.0	1.4	86
15*	5/22/99	3.46E+15	4.3	2.4	69
16	7/15/99	3.43E+16	5.0	1.1	45
17	8/9/99	9.04E+15	4.6	4.7	841
18	8/11/99	2.75E+15	4.3	2.8	55
19	9/13/99	8.54E+16	5.3	1.5	272
20*	2/11/00	6.63E+15	4.5	2.1	93
21	4/10/00	1.28E+16	4.7	1.5	42
22	6/3/00	2.82E+17	5.6	0.6	68
24	8/27/00	1.39E+16	4.7	1.9	90
25	9/29/00	3.38E+16	5.0	1.5	95
26	9/18/01	1.41E+16	4.7	1.4	32
27*	12/8/01	1.05E+16	4.6	1.7	81
29	3/13/03	3.37E+16	5.0	1.1	38

*Indicates a shallow event (hypocentral depth ≤ 30 km)

Knowing M_o, f_c, Q_o, γ, we can predict the spectra for all 150 surface sites for each event. The difference between the predicted and observed spectrum is the frequency dependent site effect. Thus we could construct the basic data set that allows us to quantify the spatial variation of the site response. With 17 deep events and 4 shallow events, we can examine the variability of the ground response from event to event as well as compare deep and shallow excitation. With 150 stations we looked at the variation from site-to-site; with 21 events (17 deep events and 4 shallow events), we can examine event-to event variations. In Figure 8, we

contoured the average site amplification (average of 17 deep events) for three frequency ranges: 0.5–1.0, 1.0–3.0 and 3-10.0 Hz. As might be expected, the low frequency (0.5–1.0 Hz) contours are fairly uniform except around stations with a large site response. In Figure 9, we have plotted average site response (ASR) by deep events versus ASV30. The least squares fits are also shown. The correlation coefficients between ASR and ASV30 for 0.5-1.0 Hz and 1.0-3.0 Hz are -0.73 and -0.58, respectively. The relationship between ASR in high frequency (3.0-10.0 Hz) and ASV30 is almost random. The data indicates that site response in a low frequency range can be statistically predictable using near-surface velocity data. Figure 10 compares the average site response from deep and shallow events. For all of the frequency range, the site responses are within the factor of two, even though the responses are calculated using completely different datasets.

Spatial Variation of Site Response

As seen in Figure 8, site response within the Yokohama array shows significant variation even for stations separated by less than 1.0 km. To examine how this site response might vary as a function of both frequency and distance we introduce a site correlation factor. Borrowing from the normal definition of correlation we define a site response correlation SRC_{ij} as

$$SRC_{ij} = \frac{2Site_i(f)Site_j(f)}{\left(Site_i(f)\right)^2 + \left(Site_j(f)\right)^2}$$

where $Site_i(f)$ is site amplification for the i^{th} station and $Site_j(f)$ is site amplification for the j^{th} station. The SRC_{ij} is normalized so that if the two site responses are identical, it will take on a maximum value of 1.0; the minimum value is 0. We looked at all pairs of stations and found 56 distinct pairs where the separation distance was less than 1.0 km (119 m – 998 m). If two pair of stations have a separation distance less than 3 m, we took the pair that had the smaller difference in the average shear wave velocity, i.e., we took the station pair that had the more similar site condition. This reduced the number of station pairs to 32. From the 32 station pairs of site response correlation we generated a contour plot of SRC_{ij} versus frequency and separation distance (Figure 11). In generating this contour plot, we smoothed over a distance of 3 m and over frequency with a 0.15 Hz interval. This plot combines spatial variability of the site amplification with frequency [29], [30]. The plot of SRC_{ij} shows that for frequencies less than ~2.0 Hz the site response is highly correlated—values of SRC_{ij} between 0.8–1.0—for all distances, up to about 600m. The site amplification for these frequencies could be generally predicted within about 20%. It is important to note that for distances 600 m and less, the average site response correlation shows a variation between 0.8 and 1.0 for all frequencies, implying that the site response could be predicted within a factor of 20%. Over all frequencies and distances the variation is generally less than a factor of 2.5; this is rather surprising to us is because we expected an even greater variation.

Future Analysis

Our next step would be to look at the probability distribution of the site response correlation as a function of distance for different frequency bands. This will enable us to estimate this probability that a spectral ordinate might vary by some pre-selected amount and of the variability one might expect in a given parameter such as PGA (f > 10 Hz) or PGV (f ~ 1–5 Hz). Another step is to consider frequency-wavenumber analysis to determine the back-azimuth of surface waves that might be excited by the deep basin structure (basin-induced surface waves).

These kinds of analysis have already been applied to seismic array data within a limited area [31], [32], [33]. However, analysis of data from this very dense array offers more possibilities of quantifying spatial variability of site response. Naturally, we intend to expand our analysis to larger separation distances and consider other methods that might shed more light on the variability of the site response, e.g., [13], [34]. A quantitative understanding of spatial variation of site response can be very helpful in predicting strong ground motion from future earthquakes.

REFERENCES

1. Reid HF. "The California earthquake of April 18, 1906." Publication 87, V21, Carnegie Institute of Washington, Washington, D.C., 1910.
2. Borcherdt RD. "Effects of local geology on ground motion near San Francisco Bay", Bull. Seism. Soc. Am. 60, 1970: 29-61.
3. Borcherdt RD, and Gibbs JF. "Effects of local geological conditions in the San Francisco Bay region on ground motions and the intensities of the 1906 earthquake." Bull. Seism. Soc. Am, 66, 1976: 467-500.
4. Hartzell S, Cranswick E, Frankel A, Carver D, and Meremonte M. "Variability of site response in the Los Angels urban area." Bull. Seism. Soc. Am. 88, 1997: 1377-1400.
5. Kawase H. "The cause of the damage belt in Kobe: the basin edge effects, constructive interference of the direct S-wave with the basin-induced diffracted/Rayleigh waves." Seism. Res. Lett. 67, 1996: 25-34.
6. Bonilla LF, Steidl JH, Lindley GT, Tumarkin AG, and Archuleta RJ. "Site amplification in the San Fernando valley, California: variability of site-effect estimation using the S-wave, coda, and H/V methods." Bull.Seism. Soc. Am. 87, 1997: 710-730.
7. Furumura T. and Koketsu K. "Specific distribution of ground motion during the 1995 Kobe earthquake and its generation mechanism." Geophys. Res. Lett, 25, 1998 785-788.
8. Stewart, J. P. and Baturay, M. B. "Uncertainties and residual in ground motion estimates at soil sites." Fourth International Conference on Recent Advances in Geotechnical Earthquake Engineering and Soil Dynamics, Shamsher P, Editor. 2001: paper 3.14.
9. Stewart, JP and Baturay, MB. "Evaluation of uncertainties in ground motion estimates for soil sites." PEER Utilities Program Report No. 2000/04, Pacific Earthquake Engineering Research Center, 2000.
10. Field EH, and the SCEC Phase III Working Group. "Accounting for site effects in probabilistic seismic hazard analyses of Southern California: Overview of the SCEC Phase III Report." Bull. Seism. Soc. Am. 90, 2000: S1-S32.
11. Abrahamson NA, Schneider JF, and Stepp JC. "Empirical spatial coherency functions for application to soil-structure interaction analyses." Earthquake Spectra, 7, 1991: 1-27.
12. Kiureghian DA "A coherency model for spatially varying ground motions." Earthquake Engng. Struc. Dyn, 25, 1996: 99-111.
13. Zerva A, and Beck JL. "Identification of parametric ground motion random fields from spatially recorded seismic data." Earthquake Engng. Struc. Dyn. 32, 2003: 771-791.
14. Zerva A, and Zhang O. "Estimation of signal characteristics in seismic ground motions." Probabilistic Eng. Mech, 11, 1996: 229-242.
15. Uetake T, and Satoh T. "Recent array experiments in Japan." Irikura, K., Kudo, K, Okada, H., Sasatani, T., Editors. Effects of Surface Geology on Seismic Motion, Vol.1, Rotterdam: AA Balkema, 1998: 51-70.
16. Torii M, Abe S, Suzuki M, Shinbo Y, Aoki T, Shintaro S, Saito M, and Midorikawa S, "Investigation for earthquake disaster mitigation using the dense strong motion network in Yokohama." Irikura, K., Kudo, K, Okada, H., Sasatani, T., Editors. Effects of Surface Geology on Seismic Motion, Vol.1, Rotterdam: AA Balkema, 1998:341-350.
17. Tsuboi S, Saito M, and Ishihara Y. "Verification of horizontal-to-vertical spectral ratio technique for estimation of the site response using borehole seismographs." Bull. Seism. Soc. Am. 91, 2001: 499-510.

18. Tsuda, K. "Inversion of ground motion spectra for site response at 150 stations of a dense accelerograph array." Master's thesis, University of Tokyo, 2001.
19. Kikuchi M, and Yamanaka Y. "EIC seismological notes." http://wwweic.eri.u-tokyo.ac.jp/EIC/EIC_News/
20. Koketsu K, and Higashi S. "Three-dimensional topography of the sediment/basement interface in the Tokyo metropolitan area, central Japan." Bull. Seism. Soc. Am. 82**,** 1992: 2328-2350.
21. Koketsu K, and Kikuchi M. "Propagation of seismic ground motion in the Kanto basin, Japan." Science. 288, 2000: 1237-1239.
22. Toshinawa T, Nishida H, Midorikawa S, and Abe S. "Comparison of spectral characteristics of strong motions and microtremors at the dense strong-motion network sites in Yokohama." Irikura, K., Kudo, K, Okada, H., Sasatani, T., Editors. Effects of Surface Geology on Seismic Motion*,* Vol.1, Rotterdam: AA Balkema, 1998: 399-406.
23. Kramer SL. "Geotechnical Earthquake Engineering, Prentice-Hall, Upper Saddle River NJ, 1996..
24. Brune JN. "Tectonic stress and the spectra of seismic shear waves from earthquakes." J. Geophys. Res., 75, 1970: 4997-5009.
25. Boatwright J. "Detailed spectral analysis of two small New York State earthquakes." Bull. Seism. Soc. Am, 68, 1978: 1117-1131.
26. Sen KM, and Stoffa PL. "Global Optimization Methods in Geophysical Inversion." Elsevier, New York, 1995.
27. Archuleta RJ, Cranswick E, Mueller C, and Spudich P. "Source parameters of the 1980 Mammoth Lakes, California, earthquake sequence." J. Geophys. Res., 87, 1982: 4595-4606.
28. Hanks TC. "Earthquake stress drops, ambient tectonic stresses and stresses that drive plate motions." Pure and Appl. Geophys., 115, 1978: 441-458.
29. Sasatani T, Higashi S, and Nagumo H. "Strong motion observations in Kushiro, Hokkaido, Japan." Irikura, K., Kudo, K, Okada, H., Sasatani, T., Editors. Effects of Surface Geology on Seismic Motion*,* Vol.1, AA Rotterdam: Balkema, 1998: 279-284.
30. Fletcher JB, Boatwright J, and Lindh AG. "Wave propagation and site response in the Santa Clara Valley." Bull. Seism. Soc. Am. 93**,** 2003: 480-500.
31. Cornou C, Bard PY, and Dietrich M. "Contribution of dense array analysis to identification and quantification of basin-edge-induced waves, Part I: Methodology." Bull. Seism. Soc. Am. **93,** no.6, 2604-2623, 2003a.
32. Cornou C, Bard PY, and Dietrich M. "Contribution of dense array analysis to identification and quantification of basin-edge-induced waves. Part II, Application to Grenoble basin (French Alps)." Bull. Seism. Soc. Am. 93**,** 2003b: 2624-2648.
33. Hartzell S, Carver D, Williams RA, Harmsen S, and Zerva A. "Site response, shallow shear-wave velocity, and wave propagation at the San Jose, California, dense seismic array." Bull. Seism. Soc. Am. 93**,** 2003: 443-464.
34. Abrahamson N, and Sykora D. "Variations of ground motions across individual sites." Proc. Fourth DOE Natural Phenomena Hazards Mitigation Conf. I, 1993: 9192-9198.

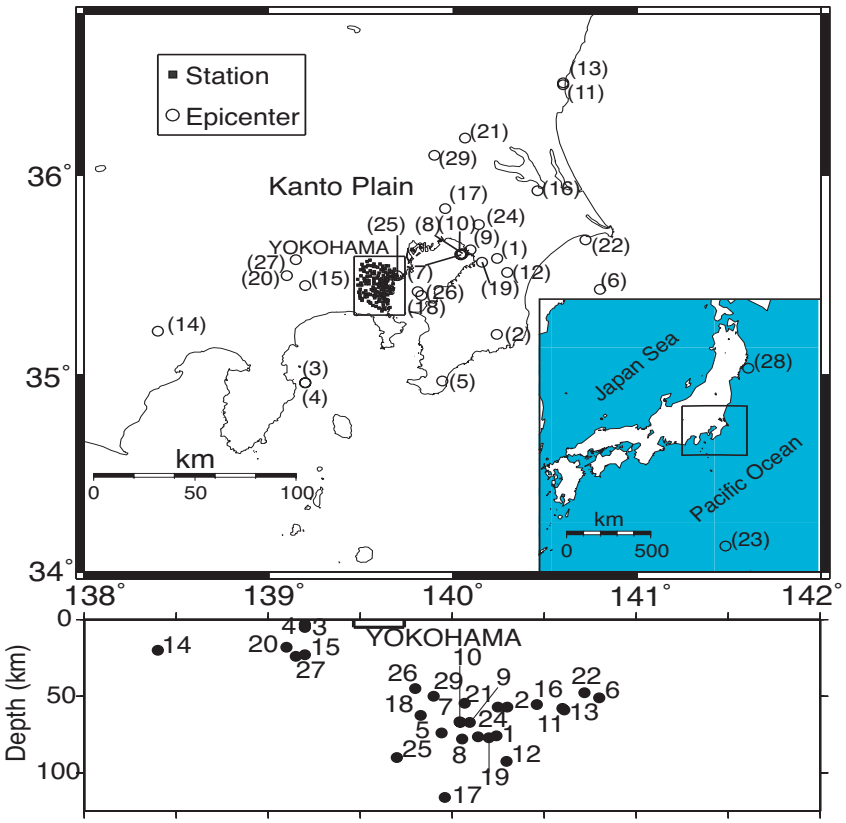

Figure 1: Distribution of epicenters and hypocenters for 29 earthquakes recorded on the 150 element array in Yokohama. Inset shows Japan and the location of the area of detail centered on Yokohama, a city with 3.4 million inhabitants.

Figure 2: A picture of installation for the surface/borehole accelerograph at each station.

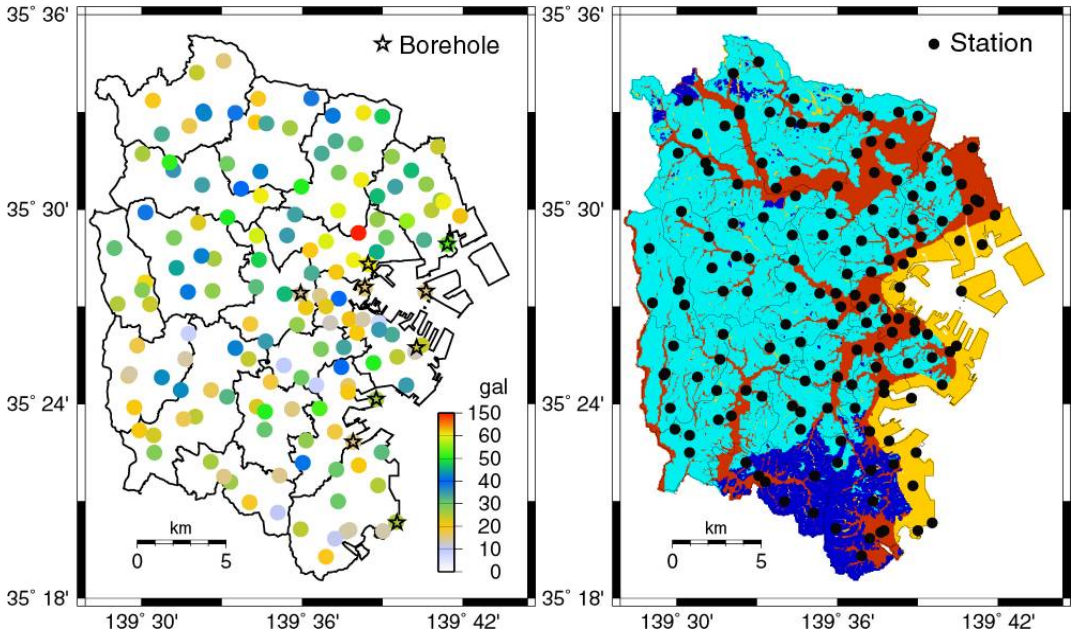

Figure 3: Left: Distribution of peak ground acceleration (PGA) from a Mw 5.3 earthquake, event # 19 in Table 1. Superposed on the outline of the city of Yokohama is the distribution of stations: surface sites (circles) and borehole sites (open stars). Right: Station locations (solid dots) are superposed on surface geology. Orange is reclaimed land; red is Holocene sediment; turquoise is Pleistocene sediment; blue is Tertiary sediment (soft rock)

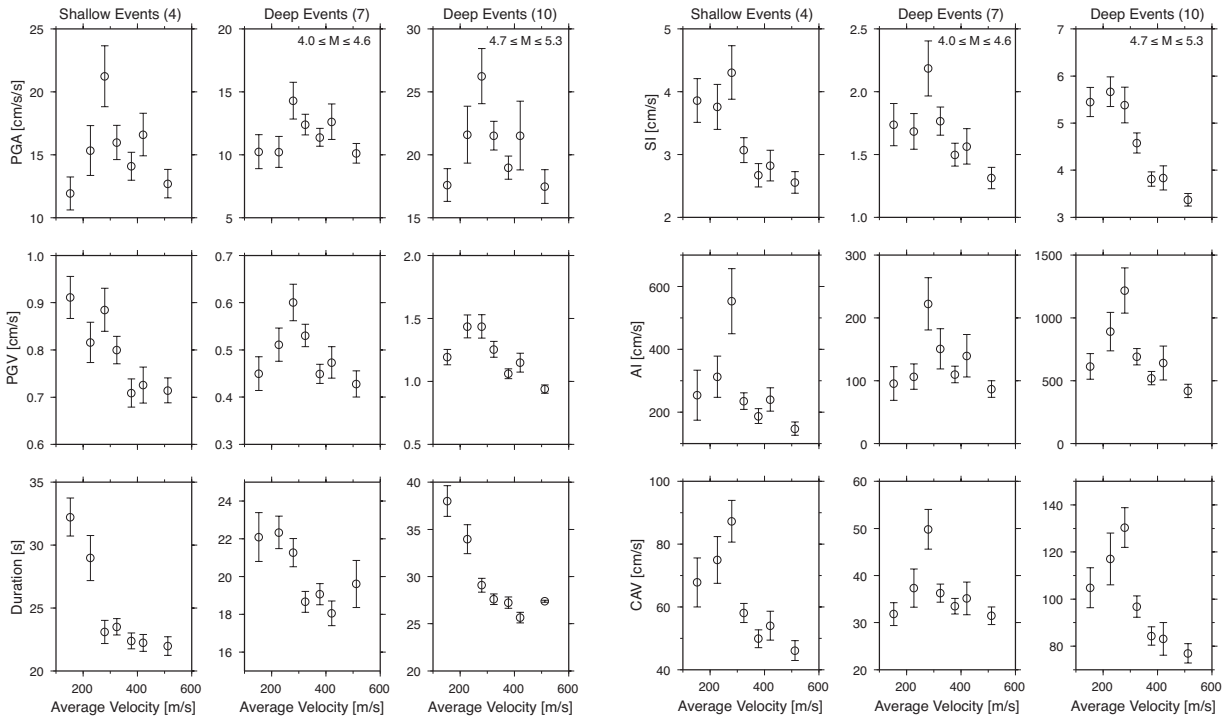

Figure 4a: Calculated spectral parameters: PGA, PGV, and Dur for the 21 events used for inversion. Each station has been binned into 7 groups based on the AVS30. 'Deep' events are divided into 2 groups with 7 events with **M** 4.0 - 4.6 and 10 events with **M** 4.7 – 5.3.
4b: Calculated spectral parameters: SI, AI and CAV for the same events.

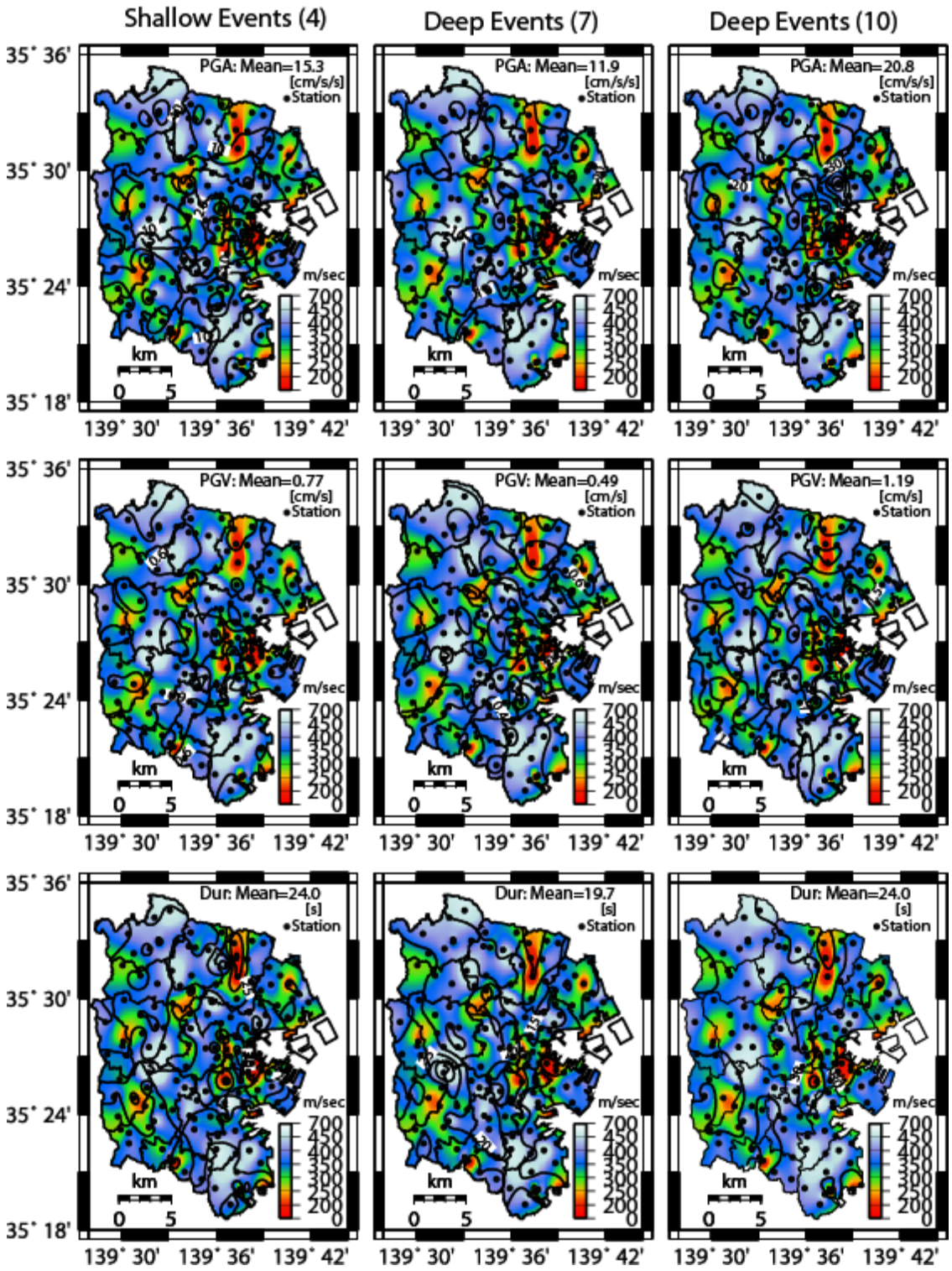

Figure 5a: Contours of PGA, PGV and DUR for the 21 events used for inversion. Each station has been binned into 7 groups based on the AVS30. 'Deep' events are divided into 2 groups with seven events with **M** 4.0 - 4.6 and 10 events with **M** 4.7 – 5.3.

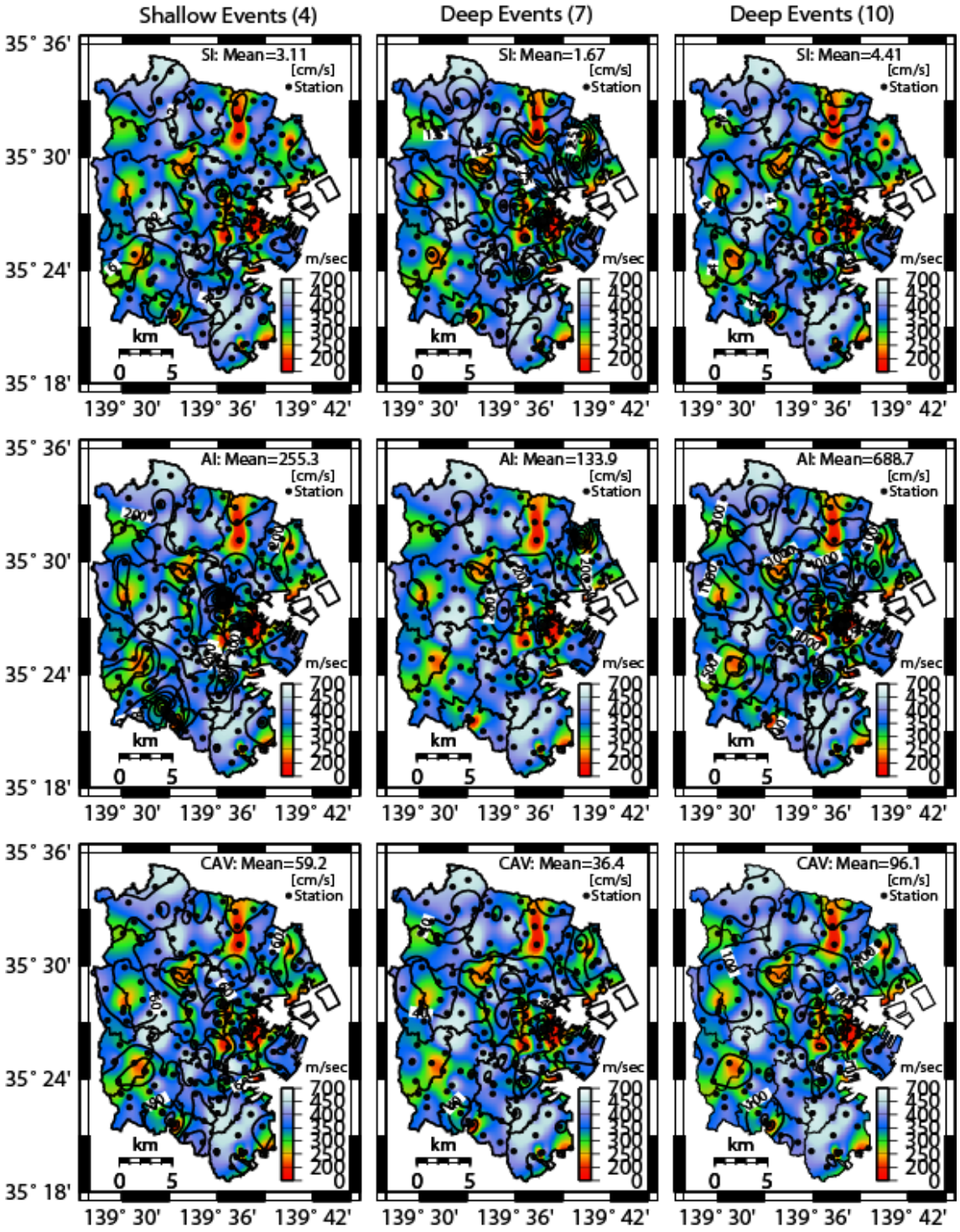

Figure 5b: Contours of SI, AI and CAV for the 21 events used for inversion. Each station has been binned into 7 groups based on the AVS30. 'Deep' events are divided into 2 groups with seven events with **M** 4.0 - 4.6 and 10 events with **M** 4.7 – 5.3.

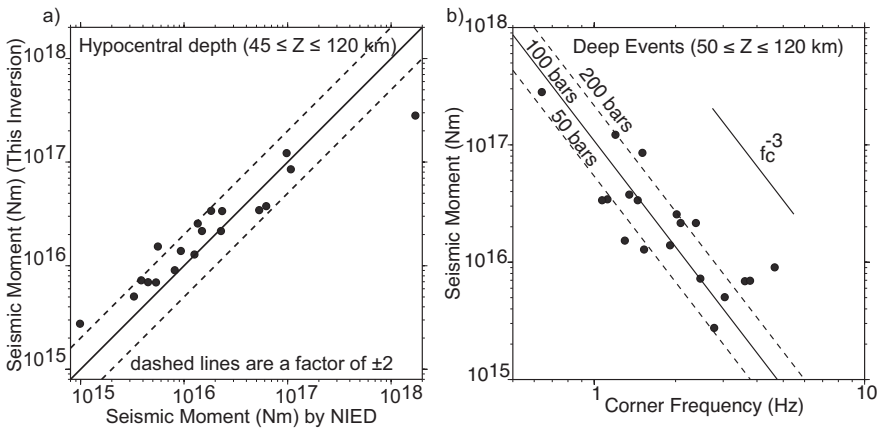

Figure 6: a) Source parameters of 17 deep events. On the left we compare our seismic moments with that originally computed by NIED using a regional broadband network in Japan. The factor of 2 is well within the norm for seismic moments. b) The plot of seismic moment vs corner frequency shows that within about a factor of 2 the stress drops are 100 bars; a factor of 2 is well below the normal scatter that is more like a factor of 10 ([27[, [28]).

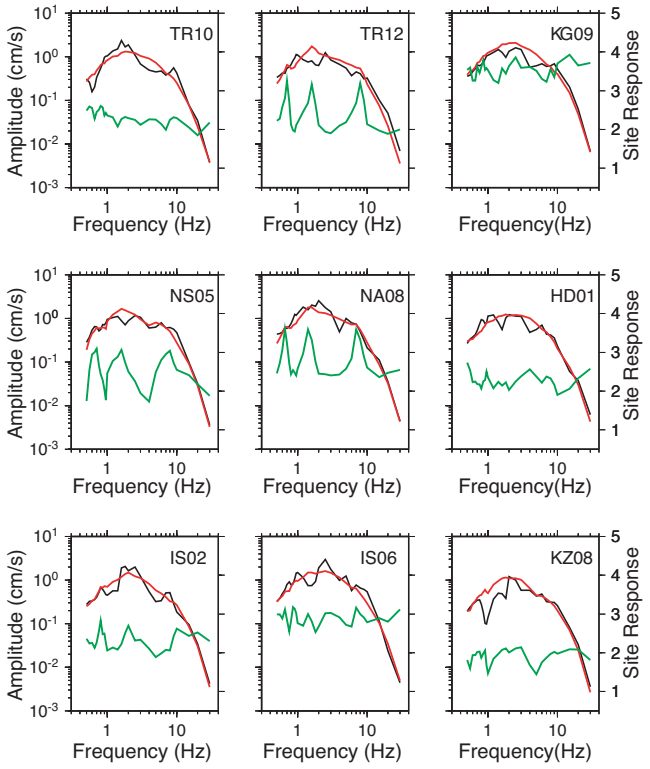

Figure 7: Predicted Fourier amplitude spectrum (red) and observed amplitude spectrum (black) taking into account a f^2 source model for Event 25 (Table 1) and path effects. The derived site response (green) is shown with a linear scale. All sites are borehole recordings; note the nearly flat response at most of the stations. However, even some of the borehole stations show resonances that we can determine through our iterative nonlinear inversion method described in the text.

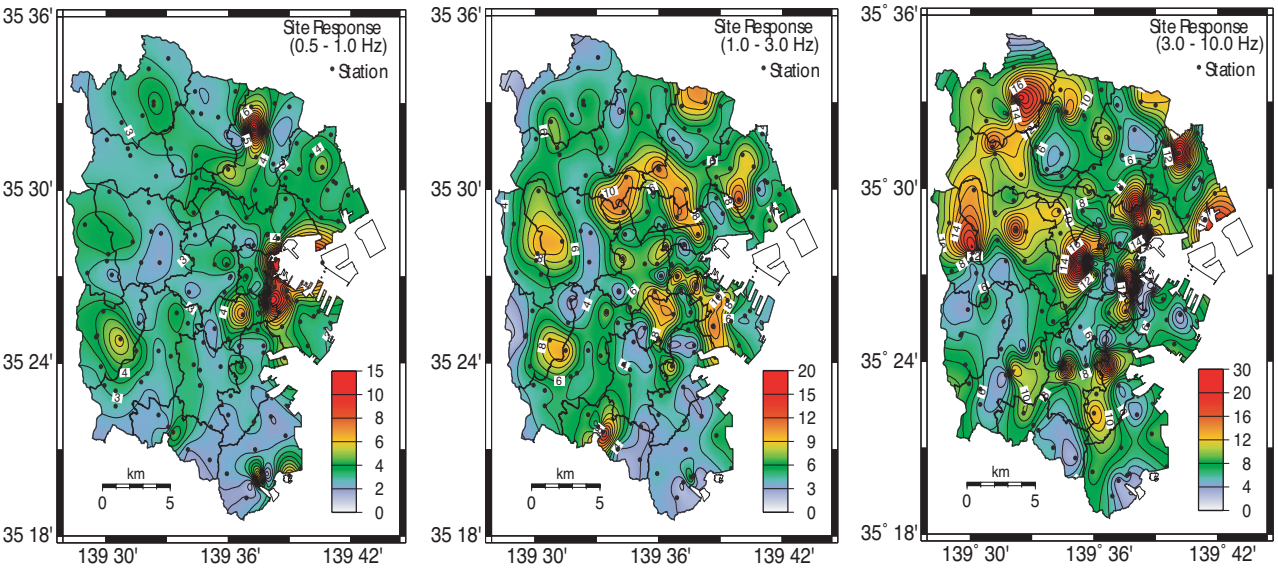

Figure 8: The mean site amplification is computed from 17 deep earthquakes. We computed average value of the site amplification in the frequency bands 0.5–1.0 Hz, 1.0–3.0 Hz and 3.0-10.0 Hz. The average amplification in these three frequency bands is contoured over the area of Yokohama. The frequency band 3.0–10.0 Hz shows broader scale amplification than the lower band even though the lower band as areas of maximum amplification.

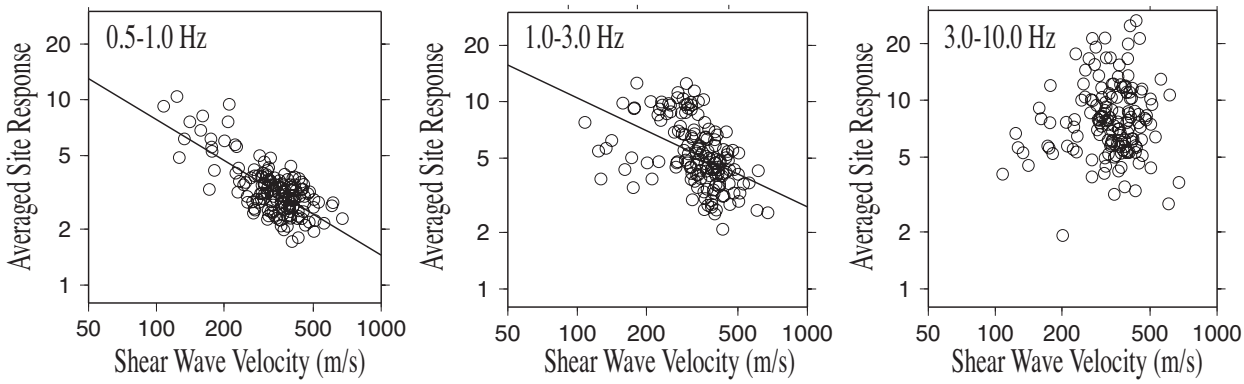

Figure 9: Distribution of the averaged site response for deep 17 events in three frequency bands: 0.5–1.0 Hz, 1.0–3.0 Hz and 3.0–10.0 Hz. The correlation coefficient, r, between V_s and Site Response is -0.72 for 0.5–1.0 Hz; 0.46 for 1.0–3.0 Hz, respectively. The solid lines are least squares fits *i.e.* representing average site response (ASR) as a function of average shear wave velocity; $ASR(V_s) = 227.5V_s^{-0.73}$ for 0.5–1.0 Hz, and $ASR(V_s) = 153.5V_s^{-0.58}$ for 1.0–3.0 Hz, respectively.

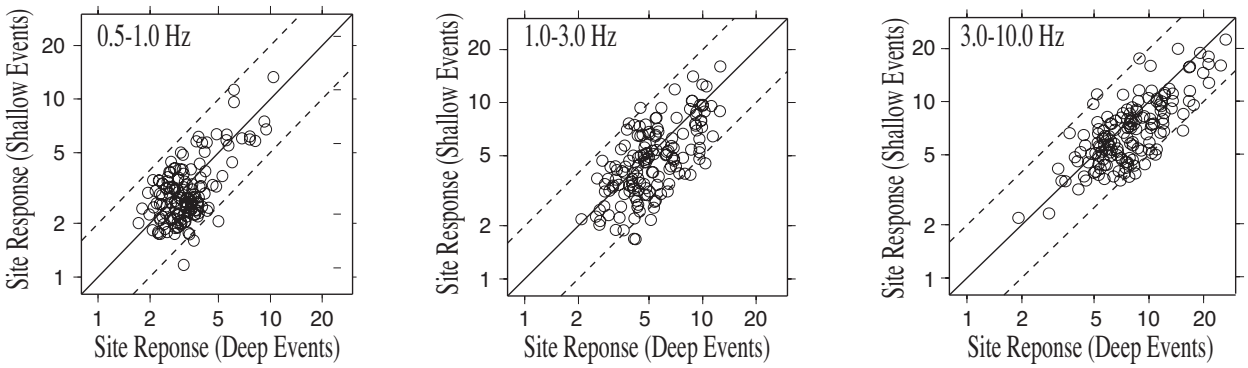

Figure 10: The comparison of the averaged site response in three frequency bands: 0.5–1.0 Hz, 1.0–3.0 Hz and 3.0–10.0 Hz. The average is based on 17 deep events and 4 shallow events. The solid line in each graph corresponds to 1:1 site response; dashed lines are a factor of ± 2.

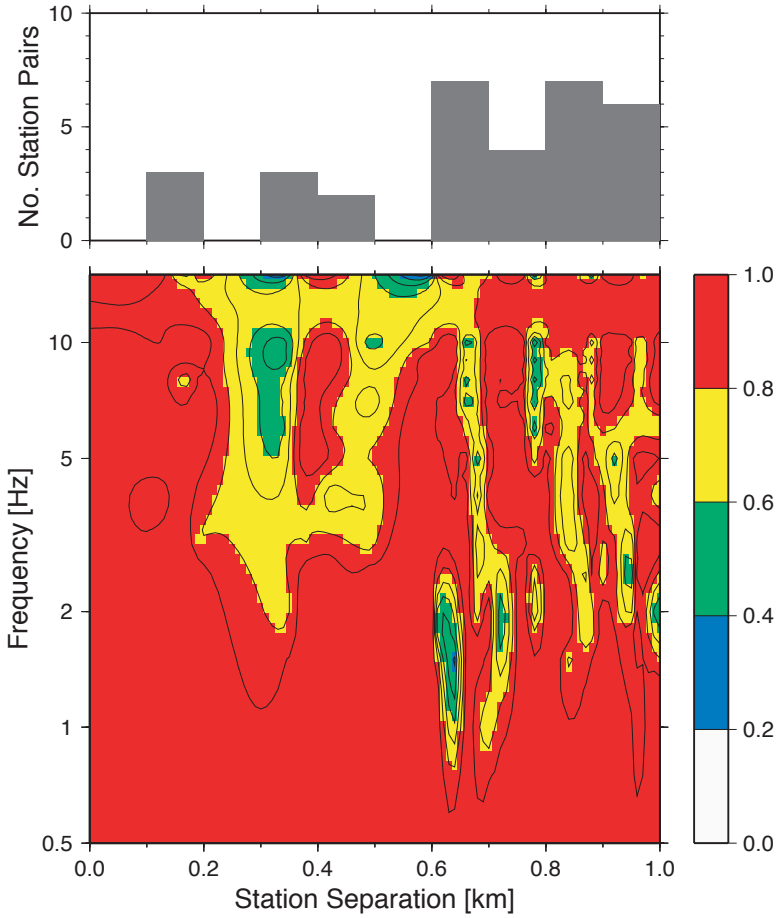

Figure 11: A contour plot generated by computing the site response correlation (see text) from 32 distinct station pairs with a separation distance between 119 m and 998 m. Note the nearly uniformly high correlation for frequencies less than about 2.0 Hz for separation distances as large as 0.6 km. Although there is more spatial variability, the site response correlation is generally more than 0.5, indicating a variation of 2.0 or less, for separation distances less than 1.0 km. As expected there is less correlation for the higher frequencies. Histogram at the top indicates the number of station pairs within 50 m intervals.